JOURNAL OF GEOPHYSICAL RESEARCH, VOL. 101, NO. B12, PAGES 28,177–28,188, DECEMBER 10, 1996

Elastodynamics of a non-ideal interface: Application to crack and fracture scattering

José M. Carcione
Osservatorio Geofisico Sperimentale, Trieste, Italy

Abstract. This work introduces a numerical algorithm for solving wave propagation in the presence of an imperfect contact between two isotropic, elastic and heterogeneous media. Non-ideal interfaces of general type can be modeled as boundary discontinuities of the displacement u and its first time derivative (the particle velocity v). The stress field is continuous, and the quantity $[\kappa u + \zeta v]$, where the brackets denote discontinuities across the interface, is equal to the corresponding stress component. The specific stiffness κ introduces frequency dependence and phase changes in the interface response. On the other hand, the specific viscosity ζ is related to the energy loss. It is shown here that, in the velocity stress formulation of the wave equation, such a model is described by Maxwell relaxation like functions. I compute the reflection and transmission coefficients in terms of the corresponding incident propagation angle and complex moduli, together with the energy dissipated at the interface. This analysis characterizes the properties of the non-ideal interface. The numerical method is based on a domain decomposition technique that assigns a different mesh to each side of the interface. As stated above, the effects of the interface on wave propagation are modeled through the boundary conditions that require a special boundary treatment based on characteristic variables. The algorithm solves the velocity-stress wave equations and two additional first-order differential equations (in two-dimensional space) in the displacement discontinuity. For each mesh, the spatial derivatives normal to the interface are solved by the Chebyshev method, and the spatial derivatives parallel to the interface are computed with the Fourier method. The algorithm allows general material variability. The modeling is applied to the problems of crack and fracture scattering.

Introduction

In seismology, exploration geophysics, and several branches of mechanics (e.g., metallurgical defects, adhesive joints, frictional contacts and composite materials), the problem of non-perfect contact between two media is of particular interest. Seismological applications include wave propagation through dry and partially saturated cracks and fractures present in the Earth's crust [*Pyrak-Nolte et al.*, 1990], which may constitute possible earthquake sources. Similarly, in oil exploration the problem finds applications in hydraulic fracturing, where a fluid is injected through a borehole to open a fracture in the direction of least principal stress. Active and passive seismic waves are used to monitor the position and geometry of the fracture [*Kleinberg et al.*, 1982; *Wills et al.*, 1992]. On the other hand, in material science, a suitable model of an imperfect interface is necessary, since strength and fatigue resistance can be degraded by subtle differences between microstructures of the interface region and the bulk material [*Mittal*, 1984; *Selvadurai and Voyiadjis*, 1986; *Murty and Kumar*, 1991].

Theories that consider imperfect bonding are mainly based on the displacement discontinuity model at the interface. Such a model was introduced by *Newmark et al.* [1951]. Later, *Mindlin* [1960] used it for the analysis of wave coupling in a plate with elastically restrained edges. *Pyrak-Nolte et al.* [1990] propose a non-welded interface model based on the discontinuity of the displacement and the particle velocity across the interface. The stress components are proportional to the displacement and velocity discontinuities through the specific stiffnesses and a specific viscosity, respectively. Displacement discontinuities conserve energy and yield frequency dependent reflection and transmission coefficients. Recent laboratory measurements [*Pyrak-Nolte et al., 1992; Hsu and Schoenberg, 1993; Pyrak-Nolte and Nolte, 1995*] confirm the predictions of the displacement discontinuity theory. On the other hand, velocity discontinuities imply an energy loss at the interface and frequency independent reflection and transmission coef-

Paper number 96JB02658.
0148-0227/96/96JB-02658$09.00

ficients. The specific viscosity accounts for the presence of a liquid under saturated conditions. The liquid introduces a viscous coupling between the two surfaces of the fracture [*Schoenberg*, 1980] and enhances energy transmission, but at the same time this is reduced by viscous losses.

A similar model to the previous one is introduced by *Murty and Kumar* [1991]. They assume two elastic half-spaces separated by a thin layer modeled by a Kelvin-Voigt medium representing a lubricant/couplant (the same model is assumed by *Carcione* [1996] to study wave propagation in reservoir environments). In the limit of small thickness (compared to the wavelength) and soft layer, they obtain a (frequency domain) displacement discontinuity boundary condition for the tangential component that resembles that of *Pyrak-Nolte et al.* [1990]. Other theories assume that the medium can be represented by a lattice with springs connecting the nearest neighbors [*Paranjape et al., 1987; Hirose and Kitahara, 1991*]. *Paranjape et al.* [1987] introduced a non-welded contact by making the springs across the interface sufficiently weaker than the springs inside the solids. A brief review of different models is given by, for instance, *Martin* [1990].

Numerical modeling of wave propagation and scattering through imperfect interfaces is relatively recent. The following works are based on low-order finite differences techniques: *Fellinger et al.* [1995] simulate the scattering produced by a crack of finite extent, subject to stress-free boundary conditions at the interface. This implies a complete decoupling of the two surfaces [*van der Hijden and Neerhoff*, 1984] which corresponds to zero stiffnesses and zero specific viscosity. *Savic and Ziolkowski* [1994] compute fracture scattering with rigid and complete slip boundary condition. In this case they set to zero the tangential stress. *Coates and Schoenberg* [1995] implement the linear deformation model (displacement discontinuity only) developed by *Schoenberg* [1980] and further used by *Pyrak-Nolte et al.* [1990] to model fractures. Finally, *Gu et al.* [1996] use a boundary element method to simulate propagation of interface waves along a fracture modeled as a displacement discontinuity.

In this work I introduce a convolutional model to account for displacement and particle velocity discontinuities at the interface. The imperfect bonding is described by four parameters: the normal and tangential specific stiffnesses and viscosities. The stiffnesses account for frequency dependent and phase change effects, and the viscosities allow for damping in the interface response. The elastodynamic equations are given in the velocity-stress formulation and the time convolutions are circumvented by introducing two first-order differential equations in the normal and tangential displacement discontinuities. A plane wave analysis gives the expressions of the reflection and transmission coefficients and the energy loss at the interface. The numerical algorithm is based on a domain decomposition technique [*Carcione*, 1991], where the implementation of the boundary conditions require a special treatment based on characteristic variables [*Carcione*, 1994].

Then, the governing equations are solved by a grid method that uses the Chebyshev differential operator normal to interface and uses the Fourier differential operator in the direction parallel to the interface.

Interface Model

Consider a planar interface in an elastic and isotropic homogeneous medium. That is, the material on both sides of the interface is the same. The non-ideal characteristics of the interface are modeled through the boundary conditions between the two half-spaces. If the displacement and stress field are continuous across the interface (ideal or welded contact), the reflection coefficient is zero and the interface cannot be detected. On the other hand, if the half-spaces are in non-ideal contact, reflected waves with appreciable amplitude can exist and the transmitted waves will be attenuated and low-pass filtered.

Assume the two-dimensional case and refer to the upper and lower half-spaces with the labels I and II, respectively, with z increasing toward the upper medium. The model proposed here is based on the discontinuity of the displacement and particle velocity fields, and continuity of stress across the interface. Then, the boundary conditions for a wave impinging on the interface ($z = 0$) are

$$[v_x] \equiv (v_x)_{II} - (v_x)_I = \psi_x * \frac{\partial \sigma_{xz}}{\partial t}, \tag{1}$$

$$[v_z] \equiv (v_z)_{II} - (v_z)_I = \psi_z * \frac{\partial \sigma_{zz}}{\partial t}, \tag{2}$$

$$(\sigma_{xz})_I = (\sigma_{xz})_{II}, \tag{3}$$

$$(\sigma_{zz})_I = (\sigma_{zz})_{II}, \tag{4}$$

where t is the time variable, v_x and v_z are the particle velocity components, σ_{xz} and σ_{zz} are the stress components, and ψ_x and ψ_z are relaxation-like functions of Maxwell type [*Christensen*, 1982] governing the tangential and normal coupling properties of the interface. The asterisk denotes time convolution. The relaxation functions can be expressed as

$$\psi_i(t) = \frac{1}{\zeta_i} \exp(-t/\tau_i) H(t), \quad \tau_i = \frac{\zeta_i}{\kappa_i}, \quad i = x \text{ or } z, \tag{5}$$

where $H(t)$ is the Heaviside function, $\kappa_x(x)$ and $\kappa_z(x)$ are specific stiffnesses, and $\zeta_x(x)$ and $\zeta_z(x)$ are specific viscosities. They have dimensions of stiffness and viscosity per unit length, respectively. The interface exhibits time dependent mechanical properties through the relaxation functions ψ_i, and, as in a viscoelastic material, implying energy dissipation.

In the frequency domain, equations (1) and (2) can be compactly rewritten as

$$[v_i] = M_i \sigma_{iz}, \quad i = x \text{ or } z, \tag{6}$$

where

$$M_i(\omega) = \mathcal{F}\left(\frac{\partial \psi_i}{\partial t}\right) = \frac{\imath\omega}{\kappa_i + \imath\omega\zeta_i} \tag{7}$$

is a specific complex modulus having dimensions of admittance (reciprocal of impedance) and ω is the angular frequency. The operator $\mathcal{F}$ performs the time Fourier transform and $\imath = \sqrt{-1}$. As is shown below, a similar model, based on combined displacement and velocity discontinuities, was developed by *Pyrak-Nolte et al.* [1990], where they introduce a single parameter (η) to describe the viscous coupling between the two surfaces of a fracture.

The characteristics of the medium are completed with the constitutive relations. Stresses and particle velocities are related by the following equations:

$$\rho\frac{\partial \sigma_{xx}}{\partial t} = {Z_P}^2\frac{\partial v_x}{\partial x} + ({Z_P}^2 - 2Z_S^2)\frac{\partial v_z}{\partial z}, \tag{8}$$

$$\rho\frac{\partial \sigma_{zz}}{\partial t} = ({Z_P}^2 - 2{Z_S}^2)\frac{\partial v_x}{\partial x} + {Z_P}^2\frac{\partial v_z}{\partial z}, \tag{9}$$

$$\rho\frac{\partial \sigma_{xz}}{\partial t} = {Z_S}^2\left(\frac{\partial v_z}{\partial x} + \frac{\partial v_x}{\partial z}\right), \tag{10}$$

where $Z_P(x,z)$ and $Z_S(x,z)$ are the compressional and shear impedances, respectively, and $\rho(x,z)$ is the material density.

In appendices A and B the reflection and transmission coefficients for incident SH and $P-SV$ waves, respectively, are derived. In addition, the energy loss at the interface is obtained.

Boundary Conditions in Differential Form

The boundary equations (1) and (2) could be implemented in a numerical solution algorithm. However, the evaluation of the convolution integrals is prohibitive when solving the differential equations with grid methods. In order to circumvent the convolutions, we recast the boundary conditions in differential form. From (1) and (2), and using convolution properties,

$$[v_i] = \frac{\partial \psi_i}{\partial t} * \sigma_{iz}. \tag{11}$$

Using (5) and after some calculation,

$$[v_i] = \psi_i(0)\sigma_{iz} - \frac{1}{\tau_i}\psi_i * \sigma_{iz}. \tag{12}$$

Since $[v_i] = \partial[u_i]/\partial t$, with u_i is the displacement field, it can be inferred from (11) that

$$[u_i] = \psi_i * \sigma_{iz}. \tag{13}$$

Then, (12) becomes

$$\frac{\partial [u_i]}{\partial t} = \frac{1}{\zeta_i}(\sigma_{iz} - \kappa_i[u_i]). \tag{14}$$

Alternatively, this equation can be written as

$$\kappa_i[u_i] + \zeta_i[v_i] = \sigma_{iz}, \tag{15}$$

which is equivalent to (17) of *Pyrak-Nolte et al.* [1990], where $\zeta_x = \eta$. Note that $\kappa_i = 0$ gives the displacement discontinuity model, and $\zeta_i = 0$ gives the particle velocity discontinuity model. On the other hand, if $\zeta_i \to \infty$ (see equation (14)), the model gives the ideal (welded) interface. As shown in the next section, (14) for $i = x$ and $i = z$ must be solved simultaneously with the equations of momentum conservation.

Domain Decomposition and Boundary Treatment

The interface model is implemented in numerical modeling by using a domain decomposition technique. *Carcione* [1991] and *Tessmer et al.* [1992] applied the method to model elastic waves across a welded interface between two elastic half-spaces and across an interface separating an acoustic layer from an elastic medium (where v_x need not be continuous). The boundary treatment is based on characteristics representing one-way waves propagating with the phase velocity of the medium. The wave equation is decomposed into outgoing and incoming wave modes perpendicular to the interface separating the two half-spaces. The outgoing waves are determined by the solution inside the corresponding half-space, while the incoming waves are calculated from the boundary conditions.

The dynamic elastic solution makes use of the equations of momentum conservation:

$$\frac{\partial v_x}{\partial t} = \frac{1}{\rho}\left(\frac{\partial \sigma_{xx}}{\partial x} + \frac{\partial \sigma_{xz}}{\partial z}\right) + f_x, \tag{16}$$

$$\frac{\partial v_z}{\partial t} = \frac{1}{\rho}\left(\frac{\partial \sigma_{xz}}{\partial x} + \frac{\partial \sigma_{zz}}{\partial z}\right) + f_z, \tag{17}$$

where f_x and f_z are the body forces. These equations together with the stress-velocity relations (8), (9), and (10), yield the velocity-stress formulation:

$$\frac{\partial \mathbf{v}}{\partial t} = \mathbf{A}\frac{\partial \mathbf{v}}{\partial x} + \mathbf{B}\frac{\partial \mathbf{v}}{\partial z} + \mathbf{f}, \tag{18}$$

where

$$\mathbf{v} = [v_x, v_z, \sigma_{xx}, \sigma_{zz}, \sigma_{xz}]^\top, \tag{19}$$

$$\mathbf{A} = \frac{1}{\rho}\begin{bmatrix} 0 & 0 & 1 & 0 & 0 \\ 0 & 0 & 0 & 0 & 1 \\ {Z_P}^2 & 0 & 0 & 0 & 0 \\ ({Z_P}^2 - 2{Z_S}^2) & 0 & 0 & 0 & 0 \\ 0 & {Z_S}^2 & 0 & 0 & 0 \end{bmatrix}, \tag{20}$$

$$\mathbf{B} = \frac{1}{\rho}\begin{bmatrix} 0 & 0 & 0 & 0 & 1 \\ 0 & 0 & 0 & 1 & 0 \\ 0 & (Z_P{}^2 - 2Z_S{}^2) & 0 & 0 & 0 \\ 0 & Z_P{}^2 & 0 & 0 & 0 \\ Z_S{}^2 & 0 & 0 & 0 & 0 \end{bmatrix}, \quad (21)$$

$$\mathbf{f} = [f_x, f_z, 0, 0, 0]^\top. \quad (22)$$

Most explicit time integration schemes compute the operation $\mathbf{Mv} \equiv (\mathbf{v})^{\text{old}}$ where

$$\mathbf{M} = \mathbf{A}\frac{\partial}{\partial x} + \mathbf{B}\frac{\partial}{\partial z}. \quad (23)$$

The vector $(\mathbf{v})^{\text{old}}$ is then updated by the boundary treatment to give a new vector $(\mathbf{v})^{\text{new}}$ that takes into account the boundary conditions.

The one-dimensional characteristic variables, perpendicular to the interface, can be obtained from the eigenvectors of matrix $\mathbf{B}$ [*Carcione, 1991; Tessmer et al., 1992*].

They are

$$P^+ = v_z + \frac{\sigma_{zz}}{Z_P}, \quad (24)$$

$$P^- = v_z - \frac{\sigma_{zz}}{Z_P}, \quad (25)$$

$$S^+ = v_x + \frac{\sigma_{xz}}{Z_S}, \quad (26)$$

$$S^- = v_x - \frac{\sigma_{xz}}{Z_S}. \quad (27)$$

$$R = Z_P{}^2\sigma_{xx} - (Z_P{}^2 - 2Z_S{}^2)\sigma_{zz}. \quad (28)$$

The first and second characteristics describe one-way compressional waves, while the third and fourth characteristics correspond to the shear wave. The last characteristic is convected toward the boundary with zero normal phase velocity. The incoming characteristics in side I are $(P^+)_I$ and $(S^+)_I$, while in side II they are $(P^-)_{II}$ and $(S^-)_{II}$. These quantities are computed from the boundary conditions at the interface, and the outgoing characteristics are left unchanged. The boundary equations can be obtained by imposing

$$(P^-)_I^{\text{new}} = (P^-)_I^{\text{old}}, \quad (29)$$

$$(S^-)_I^{\text{new}} = (S^-)_I^{\text{old}}, \quad (30)$$

$$(R)_I^{\text{new}} = (R)_I^{\text{old}}, \quad (31)$$

$$(P^+)_{II}^{\text{new}} = (P^+)_{II}^{\text{old}}, \quad (32)$$

$$(S^+)_{II}^{\text{new}} = (S^+)_{II}^{\text{old}}, \quad (33)$$

$$(R)_{II}^{\text{new}} = (R)_{II}^{\text{old}}. \quad (34)$$

These equations and the boundary conditions (1)-(4), which relate updated (new) variables, imply

$$(v_x)_I^{\text{new}} = \frac{1}{Z_S+Z_S'}\left\{Z_S'\left[(v_x)_{II}^{\text{old}} + \frac{[u_x]}{\tau_x}\right] + Z_S(v_x)_I^{\text{old}} - (\sigma_{xz})_I^{\text{old}} + (Z_S'/Z_S)(\sigma_{xz})_{II}^{\text{old}}\right\}, \quad (35)$$

$$(v_z)_I^{\text{new}} = \frac{1}{Z_P+Z_P'}\left\{Z_P'\left[(v_z)_{II}^{\text{old}} + \frac{[u_z]}{\tau_z}\right] + Z_P(v_z)_I^{\text{old}} - (\sigma_{zz})_I^{\text{old}} + (Z_P'/Z_P)(\sigma_{zz})_{II}^{\text{old}}\right\}, \quad (36)$$

$$(\sigma_{xx})_I^{\text{new}} = (\sigma_{xx})_I^{\text{old}} + \frac{Z_P{}^2-2Z_S{}^2}{Z_P{}^2}[(\sigma_{zz})_I^{\text{new}} - (\sigma_{zz})_I^{\text{old}}], \quad (37)$$

$$(\sigma_{zz})_I^{\text{new}} = \frac{Z_P'}{Z_P+Z_P'}\left\{Z_P\left[(v_z)_{II}^{\text{old}} - (v_z)_I^{\text{old}} + \frac{[u_z]}{\tau_z}\right] + (\sigma_{zz})_I^{\text{old}} + (\sigma_{zz})_{II}^{\text{old}}\right\}, \quad (38)$$

$$(\sigma_{xz})_I^{\text{new}} = \frac{Z_S'}{Z_S+Z_S'}\left\{Z_S\left[(v_x)_{II}^{\text{old}} - (v_x)_I^{\text{old}} + \frac{[u_x]}{\tau_x}\right] + (\sigma_{xz})_I^{\text{old}} + (\sigma_{xz})_{II}^{\text{old}}\right\}, \quad (39)$$

$$(v_x)_{II}^{\text{new}} = (v_x)_I^{\text{new}} + \frac{1}{\zeta_x}[(\sigma_{xz})_I^{\text{new}} - \kappa_x[u_x]], \quad (40)$$

$$(v_z)_{II}^{\text{new}} = (v_z)_I^{\text{new}} + \frac{1}{\zeta_z}[(\sigma_{zz})_I^{\text{new}} - \kappa_z[u_z]], \quad (41)$$

$$(\sigma_{xx})_{II}^{\text{new}} = (\sigma_{xx})_{II}^{\text{old}} + \frac{Z_P{}^2-2Z_S{}^2}{Z_P{}^2}[(\sigma_{zz})_{II}^{\text{new}} - (\sigma_{zz})_{II}^{\text{old}}], \quad (42)$$

$$(\sigma_{zz})_{II}^{\text{new}} = (\sigma_{zz})_I^{\text{new}}, \quad (43)$$

$$(\sigma_{xz})_{II}^{\text{new}} = (\sigma_{xz})_I^{\text{new}}, \quad (44)$$

where

$$Z_P' = \left(\frac{1}{Z_P} + \frac{1}{\zeta_z}\right)^{-1} \quad \text{and} \quad Z_S' = \left(\frac{1}{Z_S} + \frac{1}{\zeta_x}\right)^{-1}. \quad (45)$$

In the limit $\zeta_i \to \infty$, $Z_P' \to Z_P$, $Z_S' \to Z_S$, the boundary equations for a welded contact are obtained [*Carcione, 1991; Tessmer et al., 1992*].

As the specific stiffnesses and viscosities tend to zero, $Z_P' \to 0$, $Z_S' \to 0$, the solution gives the free surface boundary equations [*Carcione, 1994; Tessmer et al., 1992*]. More complex, but similar, equations can be obtained when dissimilar media are separated by the interface.

The velocity-stress equation (18) and the boundary conditions (14) are solved by a fourth-order Runge-Kutta time integration algorithm. The spatial derivatives, this is, the operation with $\mathbf{M}$ on the field variables, are computed by using the Fourier method in the horizontal direction, and the Chebyshev method in the vertical directions, where non-periodic boundary conditions are required. More details about the numerical technique are given by, for instance, *Carcione* [1992, 1994].

The procedure here is as follows: after an operation with $\mathbf{M}$, the field variables are updated by using (35)-(45); then, (14) for $i = x$ and $i = z$ is solved.

Simulations

Crack Scattering

This example considers a crack in a homogeneous medium bounded by a free surface. The medium is a Poisson solid with compressional and shear velocities $c_P = Z_P/\rho = 2000$ m/s and $c_S = Z_S/\rho = 1155$ m/s, respectively, and density $\rho = 2$ g/cm^3. The crack is at 14.6 cm from the surface and is 14.4 cm in length (see Figure 3). A distributed vertical load with a Ricker wavelet time history of central frequency $f_0 = 110$ kHz is applied at the surface. The problem is solved in the ultrasonic range, but since I consider only particle velocity discontinuities, the results can be scaled to any frequency range.

The calculations use two meshes with $N_x = 375$ and $N_z = 81$ each, and a horizontal grid spacing $D_x = 2$ mm. The vertical load is applied from grid point 132 to grid point 242 and has a length of 22 cm. The upper boundary of the model (mesh 1) has stress-free conditions, and the lower boundary (mesh 2) has open radiation conditions. At the sides, absorbing strips of length 18 grid points are used in order to eliminate wraparound effects caused by the Fourier operator. The details about the differential operators used to compute the spatial derivatives are given by, for instance, *Carcione* [1992]. The solution is propagated to 0.14 ms with a time step of 0.1 μs, by using a fourth-order Runge-Kutta integration scheme. Before introducing the crack properties I investigate the influence that the specific viscosities have on the reflection coefficients and energy loss (the equations can be found in Appendix B). Figure 1 represents the normal incidence reflection coefficient R_{PP} versus the normalized specific viscosity ζ_z/Z_P, with $\kappa_z = 0$. As can be seen, the limit $\zeta_z \to 0$ gives the complete decoupled case, and the limit $\zeta_z \to \infty$ gives the welded interface, since $R_{PP} \to 0$. The normalized energy loss for an incident compressional wave is represented in Figure 2. The maximum dissipation occurs for $\zeta_z = Z_P/2$. Similar plots and conclusions are obtained for an incident SV wave, for which the maximum loss occurs when $\zeta_x = Z_S/2$. It can be shown that, for any incident angle and values of the specific stiffnesses, there is no energy loss when $\zeta_z \to 0$ and $\zeta_z \to \infty$.

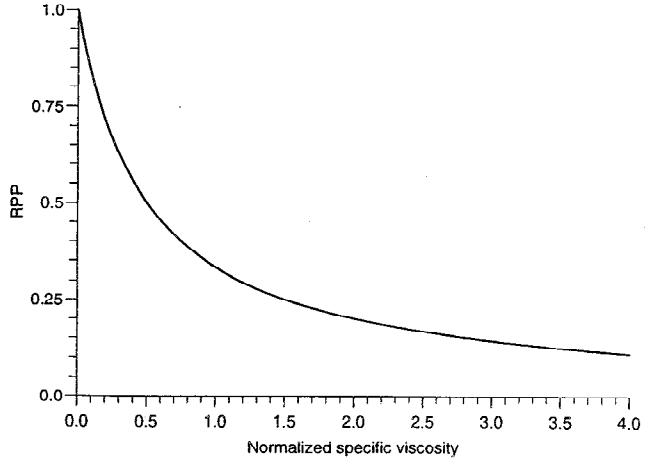

Figure 1. Normal incidence ($\theta = 0$) reflection coefficient R_{PP} versus normalized specific viscosity ζ_z/Z_P. Only the particle velocity discontinuity ($\kappa_z = 0$) has been considered. As $\zeta_z \to 0$, complete decoupling (free surface condition) is obtained. As $\zeta_z \to \infty$, the contact is welded.

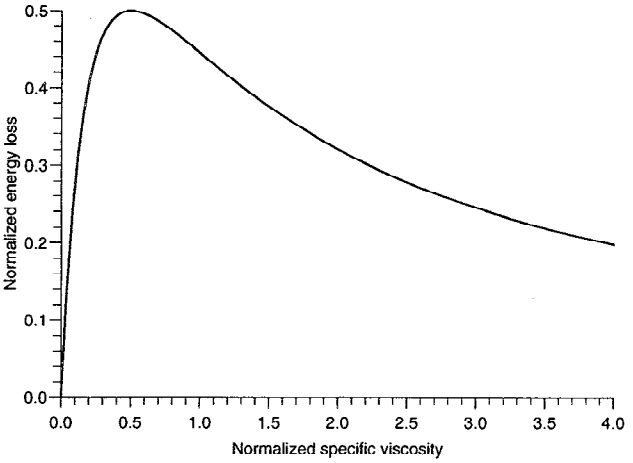

Figure 2. Normalized energy loss ϵ_{loss} at $\theta = 0$ versus normalized specific viscosity ζ_z/Z_P. A P incident wave and particle velocity discontinuity ($\kappa_z = 0$) have been considered. The maximum dissipation occurs for $\zeta_z = Z_P/2$.

I consider two cases, both with $\kappa_x = \kappa_z = 0$. In the first case, $\zeta_x = Z_S/2$ and $\zeta_z = Z_P/2$. These values give normal incidence reflection coefficients $R_{PP} = R_{SS} = 0.5$ (see Figure 1) and produce a dissipation equal to 50 % of the incident energy. Figures 3 and 4 show three snapshots of the v_x and v_z components, respectively. For visual reasons, the scales of the amplitudes in the snapshots are not the same. Indeed, the maximum amplitudes at 1 ms and 1.4 ms, for instance, are 0.78 and 0.65 relative to the maximum amplitude at 0.65 ms. The leading pulse is the compressional wave, which is followed by the shear wave. The planar fronts connecting the shear and compressional waves are the shear head waves, and, at the surface, the shear waves are followed by the Rayleigh pulses originating at the load edges. It is clear how the crack tips act as secondary sources, producing body waves. At the crack surface, the compressional wave is reflected and transmitted, and half of the energy is dissipated.

The second case has $\zeta_x = \zeta_z = 0$, hence the crack surface satisfies stress-free boundary conditions. Figure 5 represents three snapshots of the particle velocity v_z. In this case, the amplitudes are scaled with respect to the maximum amplitude at 0.65 ms. The differences from Figure 4 are that the energy is conserved and there is no transmission through the crack (see snapshot at 1 ms). Moreover, two Rayleigh waves, traveling along the crack plane, can be appreciated in the last picture.

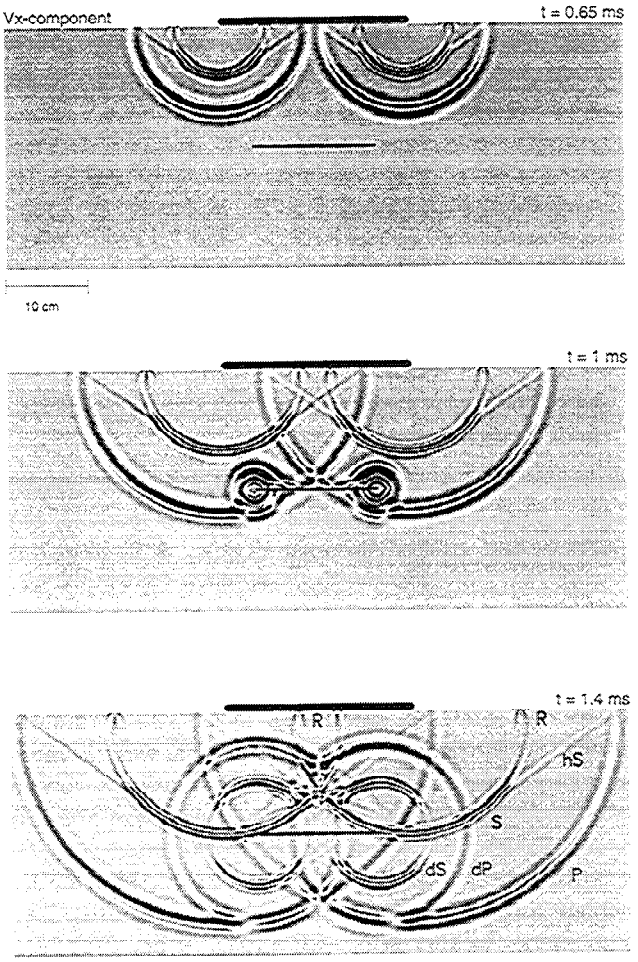

Figure 3. Vertical surface load radiation and crack scattering. The snapshots show the v_x component at different propagation times, with R, Rayleigh wave; P, compressional wave; S, shear wave; hS, head shear wave; and dP and dS, compressional and shear waves diffracted by the crack tips, respectively. The size of the model is 75 × 30 cm, and the source central frequency is 110 kHz. The specific stiffnesses and viscosities of the crack are $\kappa_x = \kappa_z = 0$, and $\zeta_x = Z_S/2$ and $\zeta_z = Z_P/2$, respectively. These values give normal incidence reflection coefficients $R_{PP} = R_{SS} = 0.5$ and produce a dissipation equal to 50 % of the incident energy.

Fracture Scattering

In this numerical experiment I study the seismic response of an infinite (ideal) fracture to a point source. The model structure is displayed in Figure 8. Its size is 6.7 km (horizontal distance) by 3 km (depth), and the fracture is situated at 1.46 km from the Earth's surface. The source is a vertical impulse of central frequency f_0 = 11 Hz, located in the left well at approximately 730 m from the surface. The medium velocities, mesh sizes and boundary conditions are the same as the previous example, and the horizontal grid spacing is D_x = 20 m. The solution is propagated to 3 s with a time step of 1 ms, by using a fourth-order Runge-Kutta integration scheme.

I consider two different fractures. The first has $\zeta_x = Z_S/2$ and $\zeta_z = Z_P/2$ and zero specific stiffnesses. Figure 6 represents the reflection and transmission coefficients for an incident compressional wave versus the incidence angle (equation (B9)). The energy loss is shown in Figure 7 (equation (B19)). As can be seen, the dissipated energy is nearly 50 % up to 80°. A snapshot of the v_z components is represented in Figure 8, where the propagation time is 1 s. The first wavefront that has crossed the fracture plane is the transmitted compressional wave, and the stronger pulse is the shear wave. Figure 9 displays two synthetic seismograms. Figure 9a is a surface seismic line, where the first receiver is located to the left of the source well, 1.48 km away, and the last receiver is located to the right of the same well, 3.72 km away. The first two hyperbolae are the direct compressional (apex at 0.36 s) and shear (0.63 s) waves. Then follow the hyperbolas corresponding to the reflected P wave (1.1 s), and reflected S wave (1.8 s). Other weaker events are the converted SP (1.4 s) and PS (1.65 s). Figure 9b is a vertical seismic profile recorded in the right well, where the first receiver is on

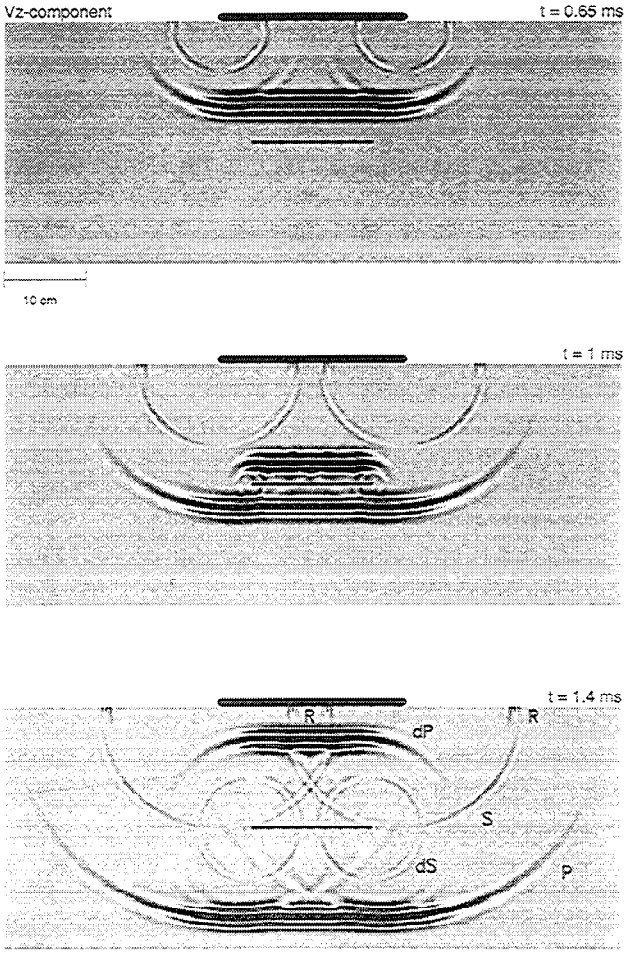

Figure 4. Vertical surface load radiation and crack scattering. The snapshots show the v_z component at differents propagation times. See caption of Figure 3 for more details.

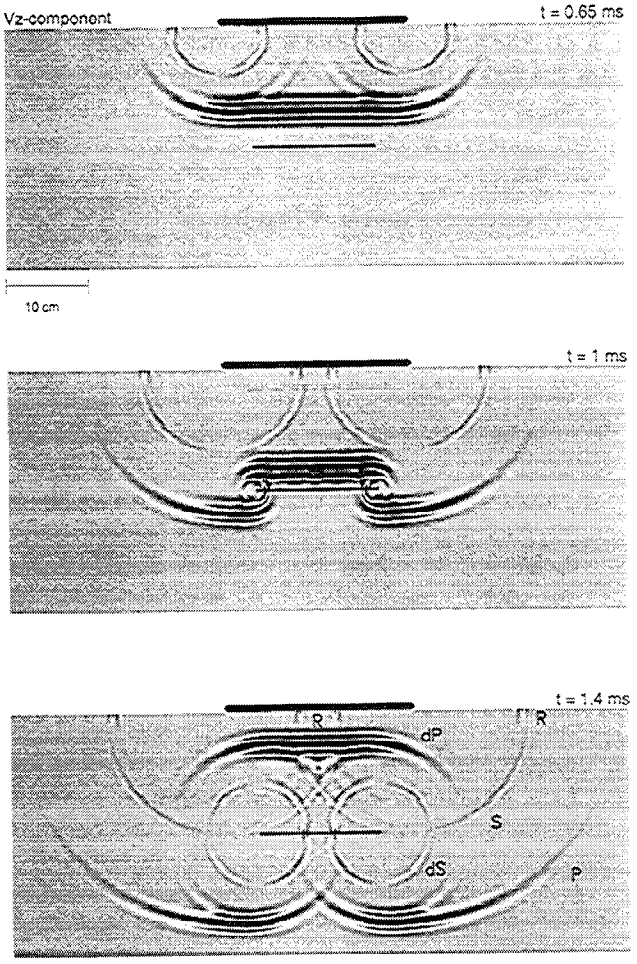

Figure 5. Vertical surface load radiation and crack scattering. The snapshots show the v_z component at differents propagation times. The size of the model is 75 × 30 cm, and the source central frequency is 110 kHz. The specific stiffnesses and viscosities of the crack are $\kappa_x = \kappa_z = 0$, and $\zeta_x = \zeta_z = 0$, respectively. These values yield a complete decoupling of the crack surfaces. See caption of Figure 3 for the identification of the different waves.

the surface and the last receiver is approximately at 3 km from the surface. The fracture plane coincides with the middle receiver. The most prominent event is the shear wave that arrives at approximately 1.7 s at the receiver located at the fracture. There, part of the energy is dissipated and the rest is reflected and transmitted. The nature of the other events can be interpreted from Figure 8.

The second fracture model has the following parameters: $\kappa_x = \pi f_0 Z_S$, $\kappa_z = \pi f_0 Z_P$, $\zeta_x = Z_S/100$ and $\zeta_z = Z_P/100$. The model is practically based on the discontinuity of the displacement field. Figure 10 represents the reflection and transmission coefficients for an incident compressional wave versus the incidence angle. In this case, the energy loss is nearly 2 % of the incident energy. That the energy is practically conserved across the fracture can be inferred by comparing Figures 8 and

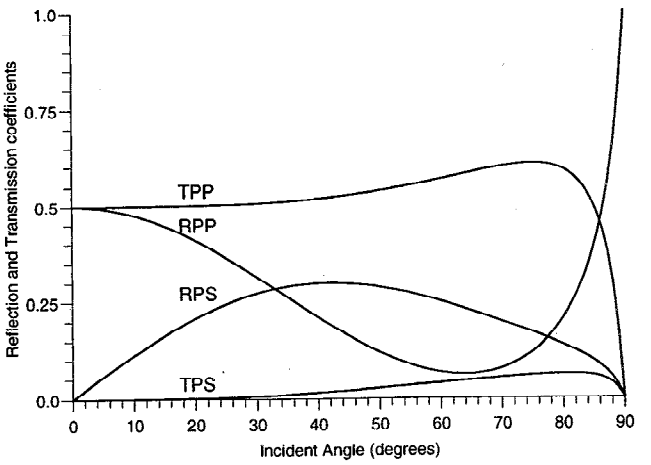

Figure 6. Reflection and transmission coefficients versus incident angle θ for a fracture defined by the following specific stiffnesses and viscosities: $\kappa_x = \kappa_z = 0$, $\zeta_x = Z_S/2$, and $\zeta_z = Z_P/2$.

11, which represent a snapshot of the v_z component at 1 s. In fact, the transmitted signal is stronger in Figure 11. Moreover, the corresponding seismograms, represented in Figures 12, show that the reflected P and S (Figure 12a) waves have a different phase compared to the same events in Figure 9a. This phenomenon is in agreement with the properties of the displacement discontinuity model.

Conclusions

A general linear model of an imperfect interface between two elastic bodies can be obtained by imposing boundary discontinuities to the displacement and particle velocity fields. This model can be expressed as a particle velocity discontinuity equal to a Maxwell relaxation function convolved with the corresponding stress component. The $P - SV$ wave propagation problem

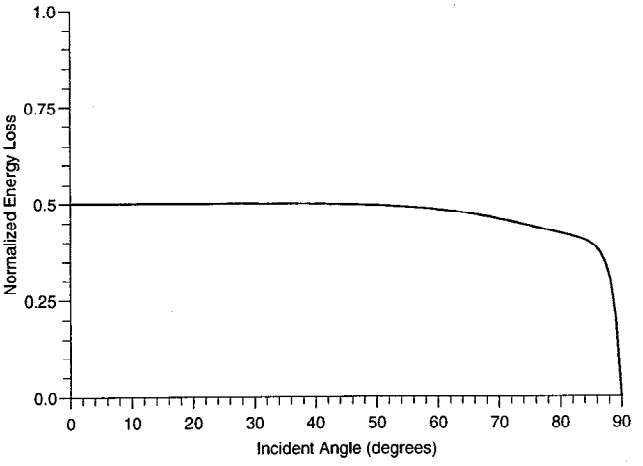

Figure 7. Normalized energy loss ϵ_{loss} versus incident angle θ for a fracture defined by the following specific stiffnesses and viscosities: $\kappa_x = \kappa_z = 0$, $\zeta_x = Z_S/2$, and $\zeta_z = Z_P/2$.

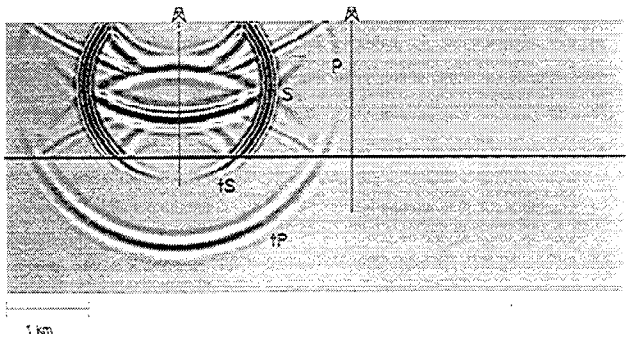

Figure 8. Snapshot of the v_z component at 1 s, with P, compressional wave, S, shear wave, tP, transmitted compressional wave and tS, transmitted shear wave. The model size is 6.7 km (horizontal distance) by 3 km (depth). The source is a vertical impulse of central frequency f_0= 11 Hz, located in the left well at approximately 730 m from the surface. The fracture parameters are given in the caption of Figure 6.

requires two specific stiffnesses and two specific viscosities, which define the properties of the non-ideal contact. The ratio viscosity to stiffness defines a relaxation time that can be associated to the response of the interface. Different choices of interface parameters give rise to the different conditions, from welded contact to stress-free boundary condition. The model allows frequency dependent reflection and transmission coefficients, phase changes, and energy dissipation.

The numerical method for solving wave propagation uses a domain decomposition technique that assigns a different mesh to each side of the interface. The use of the Chebyshev differential operator, to compute the spatial derivatives normal to the interface, allows the imposition of general boundary conditions. In particular, a boundary treatment, based on characteristic variables, implements the interface model in the velocity-stress formulation of the wave equation.

The modeling is applied to the problem of wave scattering by a crack and calculation of the seismic response of a fracture crossing two wells. The examples show how the modeling algorithm correctly simulates the influence of the non-ideal interface on the different waves, in particular, tip difractions, interface waves, partial reflection and transmission, and energy dissipation. A more precise validation of the algorithm requires the crosschecking with other modeling techniques, as, for instance, finite differencing and boundary element methods (BEM) methods.

Appendix A: Reflection and Transmission Coefficients for *SH* Waves

The simplicity of the *SH* case permits a detailed treatment of the reflection and transmission coefficients and provides some insight into the nature of energy loss in the more cumbersome $P-SV$ problem. I assume an interface separating two dissimilar materials of shear impedances Z_{SI} and Z_{SII}. The theory, corresponding to a specific stiffness κ_y and a specific viscosity ζ_y, satisfies the following boundary conditions:

$$(v_y)_{II} - (v_y)_I = \psi_y * \frac{\partial \sigma_{yz}}{\partial t}, \tag{A1}$$

$$(\sigma_{yz})_I = (\sigma_{yz})_{II}, \tag{A2}$$

where

$$\rho \sigma_{yz} = Z_S^2 \frac{\partial u_y}{\partial z}, \tag{A3}$$

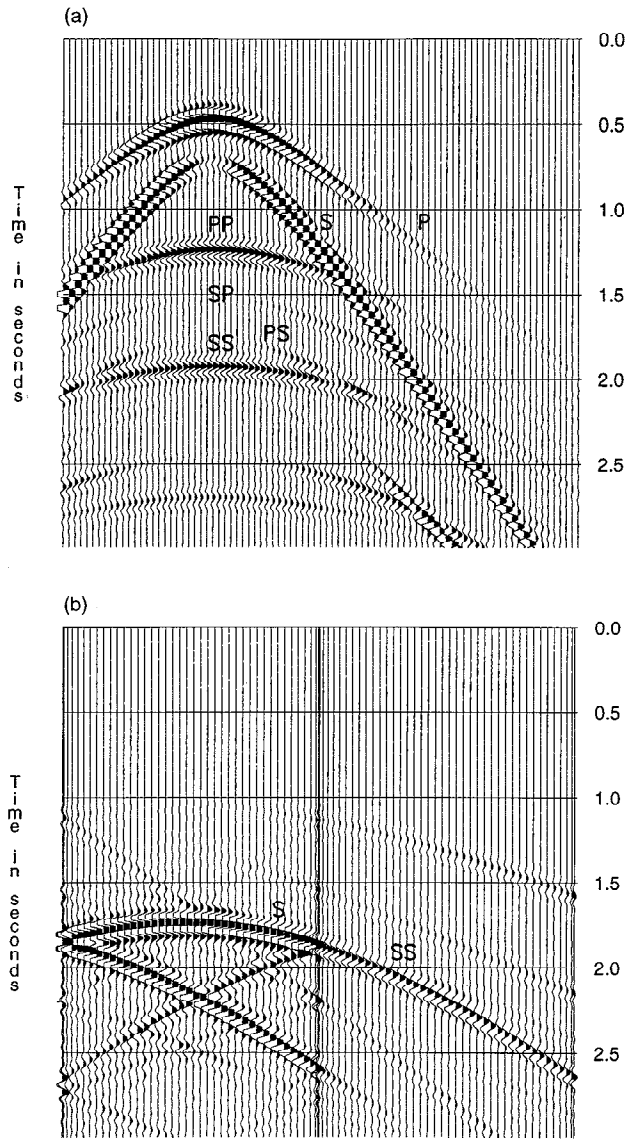

Figure 9. Synthetic seismograms corresponding to the numerical experiment shown in Figure 8. A surface seismogram is represented in Figure 9a. The first receiver is located to the left of the source well, 1.48 km away, and the last receiver is located to the right of the same well, 3.72 km away. The direct and reflected events are indicated in the figure. A vertical seismic profile is shown in Figure 9b. The first receiver is on the surface and the last receiver is at approximately 3 km from the surface. In this case, SS represents the transmitted shear wave (tS in Figure 8).

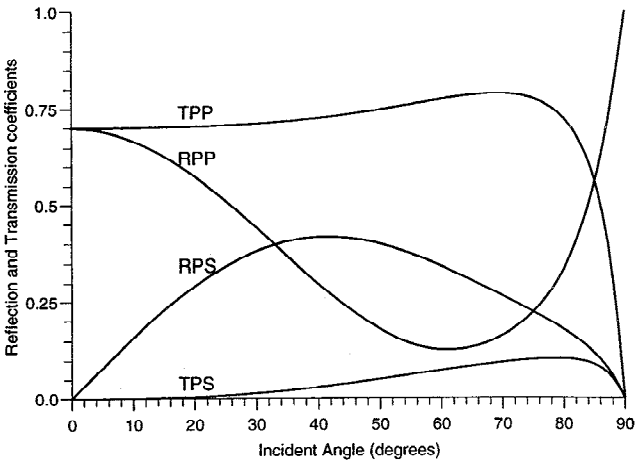

Figure 10. Reflection and transmission coefficients versus incident angle θ for a fracture defined by the following specific stiffnesses and viscosities: $\kappa_x = \pi f_0 Z_S$ and $\kappa_z = \pi f_0 Z_P$, and $\zeta_x = Z_S/100$ and $\zeta_z = Z_P/100$, where f_0 is the source central frequency.

and u_y is the displacement field. The relaxation function ψ_y has the same form given in (5) with $i = y$.

In half-space I, the field is

$$(u_y)_I = \exp[\imath k_{SI}(x\sin\theta + z\cos\theta)] + R\exp[\imath k_{SI}(x\sin\theta - z\cos\theta)], \quad \text{(A4)}$$

where k_{SI} is the wavenumber and R is the reflection coefficient. In half-space II, the displacement field is

$$(u_y)_{II} = T\exp[\imath k_{SII}(x\sin\delta + z\cos\delta)], \quad \text{(A5)}$$

where T is the transmission coefficient and

$$\delta = \arcsin[(k_{SI}/k_{SII})\sin\theta],$$

according to Snell's law. For clarity, the factor $\exp(-\imath\omega t)$ has been omitted in (A4) and (A5).

Considering that $v_y = -\imath\omega u_y$, the reflection and transmission coefficients are obtained by substituting the displacements into the boundary conditions. This gives

$$R = \frac{Y_I - Y_{II} + Z}{Y_I + Y_{II} + Z}, \qquad T = \frac{2Y_I}{Y_I + Y_{II} + Z}, \quad \text{(A6)}$$

where

$$Y_I = Z_{SI}\cos\theta, \quad Y_{II} = Z_{SII}\cos\delta, \quad \text{(A7)}$$

$$Z(\omega) = Y_I Y_{II} M_y(-\omega), \quad \text{(A8)}$$

and the relation $k_{SI(II)}Z_{SI(II)} = \rho\omega$ has been used.

Since

$$M_y(\omega) = \frac{\imath\omega}{\kappa_y + \imath\omega\zeta_y}, \quad \text{(A9)}$$

the reflection and transmission coefficients are frequency independent for $\kappa_y = 0$ and, moreover, there are no phase changes. In this case, when $\zeta_y \to 0$, $R \to 1$ and $T \to 0$, and the free surface condition is obtained; when $\zeta_y \to \infty$, $R \to 0$ and $T \to 1$, giving an ideal welded interface.

In a completely welded interface, the normal component of the mean energy flux is continuous across the plane separating the two media [*Borcherdt*, 1977].

This is a consequence of the boundary conditions that impose continuity of normal stress and particle velocity. The normal component of the mean energy flux is proportional to the real part of $\sigma_{yz}v_y^*$ [e.g., *Carcione and Cavalini*, 1993], where an asterisk denotes complex conjugate. Since the media are elastic, the interference terms between different waves vanish, and only the fluxes corresponding to each single beam need be considered. After normalizing with respect to the incident wave, the reflected and transmitted energy fluxes are

$$\text{reflected wave} \to |R|^2, \quad \text{(A10)}$$

$$\text{transmitted wave} \to \frac{Y_{II}}{Y_I}|T|^2. \quad \text{(A11)}$$

The energy loss at the interface is obtained by substracting the reflected and transmitted energies from the incident energy. The normalized dissipated energy is

$$\epsilon_{\text{loss}} = 1 - |R|^2 - \frac{Y_{II}}{Y_I}|T|^2. \quad \text{(A12)}$$

Substituting the reflection and transmission coefficients the energy loss becomes

$$\epsilon_{\text{loss}} = \frac{4Y_{II}Z_R}{(Y_I + Y_{II} + Z_R)^2 + Z_I^2}, \quad \text{(A13)}$$

where Z_R and Z_I are the real and imaginary parts of Z, given by

$$Z_R = \frac{\omega^2\zeta_y Y_I Y_{II}}{\kappa_y^2 + \omega^2\zeta_y^2}, \qquad Z_I = \frac{\omega\kappa_y Y_I Y_{II}}{\kappa_y^2 + \omega^2\zeta_y^2}. \quad \text{(A14)}$$

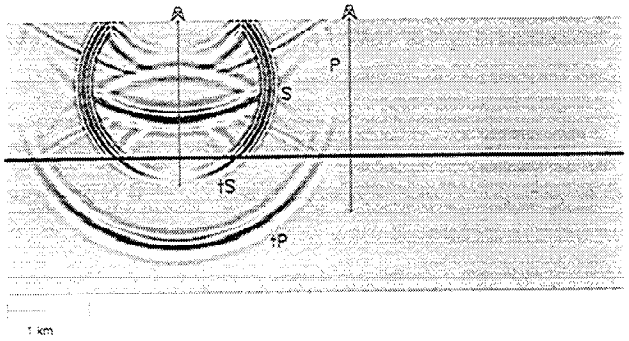

Figure 11. Snapshot of the v_z component at 1 s. The model size is 6.7 km (horizontal distance) by 3 km (depth). The source is a vertical impulse of central frequency f_0= 11 Hz, located in the left well at approximately 730 m from the surface. The fracture parameters are given in the caption of Figure 10. See caption of Figure 8 for the identification of the different waves.

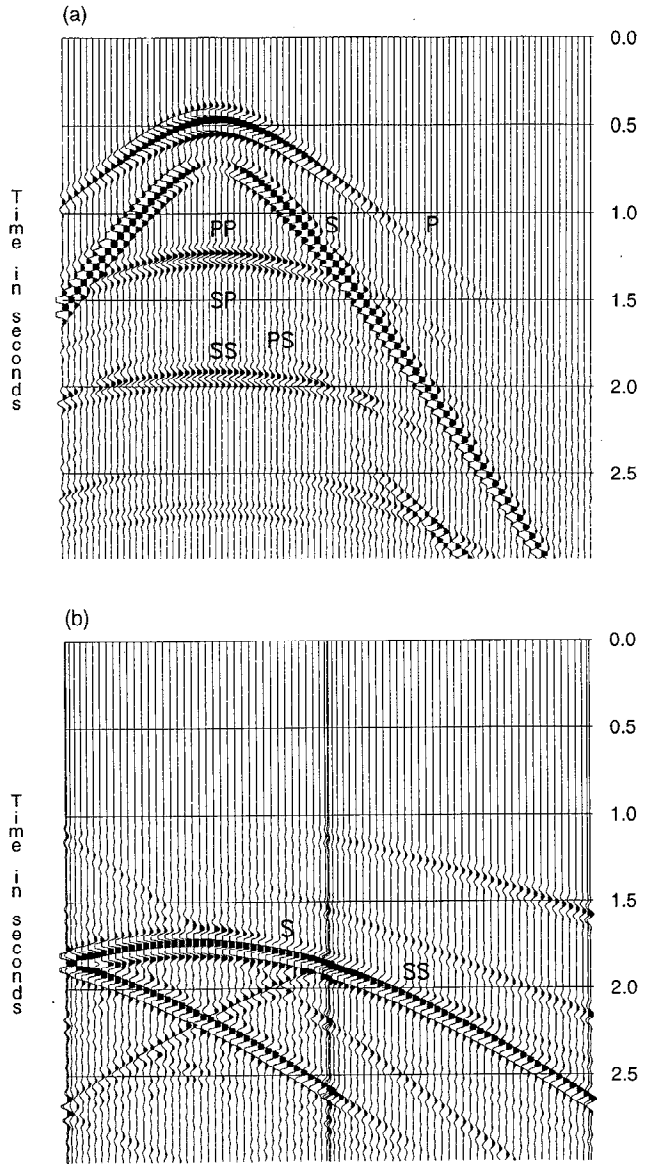

Figure 12. Synthetic seismograms corresponding to the numerical experiment shown in Figure 11. Figures 12a and 12b represent a surface seismogram and a vertical seismic profile, respectively, whose spatial configurations and wave identification are given in the caption of Figure 9.

If $\kappa_y = 0$, $Z_I = 0$, $Z_R = Y_I Y_I I/\zeta_y$, and the energy loss is frequency independent. When $\zeta_y \to 0$ (complete decoupling) and $\zeta_y \to \infty$ (welded contact), there is no energy dissipation.

If $\kappa_y = 0$, the maximum loss is obtained for

$$\zeta_y = \frac{Y_I Y_{II}}{Y_I + Y_{II}}. \tag{A15}$$

At normal incidence and equal lower and upper media, this gives $\zeta_y = Z_S/2$, and a (normalized) energy loss $\epsilon_{\text{loss}} = 0.5$, that is, half of the normally incident energy is dissipated at the interface.

Appendix B: Reflection and Transmission Coefficients for $P - SV$ Waves

Consider an interface separating two half-spaces with equal material properties, where the boundary conditions are given by (1)-(4). Application of Snell's law indicates that the transmitted angle is equal to the incident angle and that

$$k_P \sin\theta = k_S \sin\alpha,$$

where k_P and k_S are the wavenumbers of the compressional and shear waves, and θ and α are the respective associated angles. The boundary conditions do not influence the emergence angles of the transmitted and reflected waves.

In terms of the dilatational and shear potentials ϕ and ψ, the displacements are given by

$$u_x = \frac{\partial\phi}{\partial x} - \frac{\partial\psi}{\partial z}, \qquad u_z = \frac{\partial\phi}{\partial z} + \frac{\partial\psi}{\partial x}, \tag{B1}$$

and the stress components by [*Pilant*, 1979].

$$\sigma_{xz} = \frac{Z_S^2}{\rho}\left(2\frac{\partial^2\phi}{\partial x\partial z} + \frac{\partial^2\psi}{\partial x^2} - \frac{\partial^2\psi}{\partial z^2}\right), \tag{B2}$$

$$\sigma_{zz} = \frac{Z_P^2}{\rho}\left(\frac{\partial^2\phi}{\partial x^2} + \frac{\partial^2\phi}{\partial z^2}\right) - \frac{2Z_S^2}{\rho}\left(\frac{\partial^2\phi}{\partial x^2} - \frac{\partial^2\psi}{\partial x\partial z}\right). \tag{B3}$$

I consider a compressional wave incident from half-space I. Then, the incident and reflected potentials are

$$\phi_0 = \exp[\imath k_P(x\sin\theta + z\cos\theta)], \tag{B4}$$

$$\phi_R = R_{PP}\exp[\imath k_P(x\sin\theta - z\cos\theta)], \tag{B5}$$

$$\psi_R = R_{PS}\exp[\imath k_S(x\sin\alpha - z\cos\alpha)]. \tag{B6}$$

On the other hand, in half-space II, the transmitted potentials are

$$\phi_T = T_{PP}\exp[\imath k_P(x\sin\theta + z\cos\theta)], \tag{B7}$$

$$\psi_T = T_{PS}\exp[\imath k_S(x\sin\alpha + z\cos\alpha)]. \tag{B8}$$

Considering that $v_x = -\omega u_x$ and $v_z = -\omega u_z$, the solution for an incident P wave is

$$\begin{bmatrix} s_\alpha\left(1 + 2\gamma_x\frac{ZS}{ZP}c_\theta\right) & c_\alpha + \gamma_x c_{2\alpha} & -s_\alpha & c_\alpha \\ -\gamma_z c_{2\alpha} - c_\theta & s_\theta + \gamma_z s_{2\alpha} & -c_\theta & -s_\theta \\ 2\frac{ZS}{ZP}s_\alpha c_\theta & c_{2\alpha} & 2\frac{ZS}{ZP}s_\alpha c_\theta & -c_{2\alpha} \\ -c_{2\alpha} & s_{2\alpha} & c_{2\alpha} & s_{2\alpha} \end{bmatrix} \times \begin{bmatrix} R_{PP} \\ R_{PS} \\ T_{PP} \\ T_{PS} \end{bmatrix} = \begin{bmatrix} -s_\alpha\left(1 - 2\gamma_x\frac{ZS}{ZP}c_\theta\right) \\ \gamma_z c_{2\alpha} - c_\theta \\ 2\frac{ZS}{ZP}s_\alpha c_\theta \\ c_{2\alpha} \end{bmatrix}, \tag{B9}$$

where

$$\gamma_x = Z_S M_x(-\omega), \qquad \gamma_z = Z_P M_z(-\omega), \tag{B10}$$

and the following relations have been used:

$$Z_S k_S = \rho\omega, \qquad Z_P k_P = \rho\omega, \tag{B11}$$

$$\rho\mu = Z_S^2, \qquad \rho\lambda = Z_P^2 - 2Z_S^2. \tag{B12}$$

The abbreviations $s_\epsilon = \sin\epsilon$ and $c_\epsilon = \cos\epsilon$ are used in equation (B9).

The reflection and transmission coefficients for a P wave at normal incidence are

$$R_{PP} = -\left(1 + \frac{2}{\gamma_z}\right)^{-1} \tag{B13}$$

$$T_{PP} = \left(1 + \frac{\gamma_z}{2}\right)^{-1}, \tag{B14}$$

respectively. If $\zeta_z = 0$, the coefficients given by *Pyrak-Nolte et al.* [1990] are obtained. If, moreover, $\kappa_z \to 0$, $R_{PP} \to -1$ and $T_{PP} \to 0$, and the free surface condition is obtained; when $\zeta_z \to \infty$, $R_{PP} \to 0$ and $T_{PP} \to 1$, giving the solution for a welded contact. On the other hand, it can be seen that $\zeta_z = 0$ and $\kappa_z = \omega Z_P/2$ gives $|R|^2 = 1/2$. The characteristic frequency $\omega_P \equiv 2\kappa_z/Z_P$ defines the transition from the apparently perfect interface to the apparently delaminated one [*Nagy and Adler*, 1990]. The reflection and transmission coefficients corresponding to an incident SV wave can be obtained in the same way as for the incident P wave. In particular, the normal incident coefficients R_{SS} and T_{SS} have the same form as (B13) and (B14) but substituting γ_z by γ_x.

Following the same procedure to obtain the energy flow in the SH case, we get the following normalized energies for an incident P wave:

$$\text{reflected } P \text{ wave} \to |R_{PP}|^2, \tag{B15}$$

$$\text{reflected } S \text{ wave} \to \frac{\tan\theta}{\tan\alpha}|R_{PS}|^2, \tag{B16}$$

$$\text{transmitted } P \text{ wave} \to |T_{PP}|^2, \tag{B17}$$

$$\text{transmitted } S \text{ wave} \to \frac{\tan\theta}{\tan\alpha}|T_{PS}|^2. \tag{B18}$$

Hence the normalized energy loss is

$$\epsilon_{\text{loss}} = 1 - |R_{PP}|^2 - |T_{PP}|^2 - \frac{\tan\theta}{\tan\alpha}(|R_{PS}|^2 + |T_{PS}|^2). \tag{B19}$$

It can be easily shown that the amount of dissipated energy at normal incidence is

$$\epsilon_{\text{loss}} = \frac{4\gamma_{zR}}{(2+\gamma_{zR})^2 + \gamma_{zI}^2}, \tag{B20}$$

where the subindices R and I denote real and imaginary parts, respectively. If $\kappa_z = 0$, the maximum loss is obtained for $\zeta_z = Z_P/2$. Similarly, if $\kappa_x = 0$, the maximum loss for an incident SV wave occurs when $\zeta_x = Z_S/2$.

Acknowledgments. This work was funded in part by AGIP S.p.A. and the European Commission in the framework of the JOULE programme, sub-programme Advanced Fuel Technologies. Thanks to Giorgio Padoan for helping with the word processing.

References

Borcherdt, R. D., Reflection and refraction of type-II S waves in elastic and anelastic media, *Bull. Seismol. Soc. Am.*, *67*, 43-67, 1977.

Carcione, J. M., Domain decomposition for wave propagation problems, *J. Sci. Comput.*, *6*, 453-472, 1991.

Carcione, J. M., Modeling anelastic singular surface waves in the Earth, *Geophysics*, *57*, 781-792, 1992.

Carcione, J. M., Time-dependent boundary conditions for the 2-D linear anisotropic-viscoelastic wave equation, *Numer. Methods Part. Diff. Equations*, *10*, 772-791, 1994.

Carcione, J. M., Plane-layered models for the analysis of wave propagation in reservoir environments, *Geophys. Prospect.*, *44*, 3-26, 1996.

Carcione, J. M., and F. Cavallini, Energy balance and fundamental relations in anisotropic-viscoelastic media, *Wave Motion*, *18*, 11-20, 1993.

Christensen, R. M., *Theory of Viscoelasticity, An Introduction*, Academic, San Diego, Calif., 1982.

Coates, R. T., and M. Schoenberg, Finite difference modeling of faults and fractures, *Geophysics*, *60*, 1514-1526, 1995.

Fellinger, P., R. Marklein, K. J. Langenberg and S. Klaholz, Numerical modeling of elastic wave propagation and scattering with EFIT - elastodynamic finite integration technique, *Wave Motion*, *21*, 47-66, 1995.

Gu, B., K. T. Nihei, L. R. Myer and L. J. Pyrak-Nolte, Fracture interface waves, *J. Geophys. Res. 101*, 827-835, 1996.

Hirose, S., and M. Kitahara, Scattering of elastic wave by a crack with spring-mass contact, *Int. J. Numer. Methods Eng.*, *31*, 789-801, 1991.

Hsu, C. J., and M. Schoenberg, Elastic waves through a simulated fractured medium, *Geophysics*, *58*, 964-977, 1993.

Kleinberg, R. L., E. Y. Chow, T. J. Plona, M. Orton, and W. J. Canady, Sensitivity and reliability of fracture detection techniques for borehole application, *J. Pet. Technol. 34*, 657-663, 1982.

Martin, P. A., Thin interface layers, adhesives, approximations and analysis, in *Elastic Waves and Ultrasonic Nondestructive Evaluations*, edited by S. K. Datta, J. D. Achenbach, and Y. S. Rajapakse, pp. 217-222, Elsevier Sci., New York, 1990.

Mindlin, R. D., Waves and vibrations in isotropic elastic planes, in *Structural Mechanics*, edited by J. W. Goodier and W. J. Hoff, p. 199, Pergamon, Tarrytown, N. Y., 1960.

Mittal, K. L. (Ed.), *Adhesive Joints*, Plenum, New York (1984).

Murty, G. S., and V. Kumar, Elastic wave propagation with kinematic discontinuity along a non-ideal interface between two isotropic elastic half-spaces, *J. Nondestr. Eval.*, *10*, 39-53 (1991).

Nagy, P. B., and L. Adler, New ultrasonic techniques to evaluate interfaces, in *Elastic Waves and Ultrasonic Nondestructive Evaluations*, edited by S. K. Datta, J. D. Achenbach, and Y. S. Rajapakse, pp. 229-239, Elsevier Sci., New York, 1990.

Newmark, N. M., C. P. Siess, and I. M. Viest, Test and analysis of composite beams with incomplete interaction, *Proc. Soc. Exp. Stress Anal.*, *9*, 75-92, 1951.

Paranjape, B. V., N. Arimitsu, and E. S. Krebes, Reflection and transmission of ultrasound from a planar interface, *J. Appl. Phys.*, *61*, 888-894, 1987.

Pilant, W. L., *Elastic Waves in the Earth*, Elsevier, New York, 1979.

Pyrak-Nolte, L. J., and D. D. Nolte, Wavelet analysis of velocity dispersion of elastic interface waves propagating along a fracture, *Geophys. Res. Lett.*, *22*, 1329-1332, 1995.

Pyrak-Nolte, L. J., L. R. Myer, and N. G. W. Cook, Transmission of seismic waves across single natural fractures, *J. Geophys. Res.*, *95*, 8617-8638, 1990.

Pyrak-Nolte, L. J., J. Xu, and G. M. Haley, Elastic interface waves propagating in a fracture, *Phys. Rev. Lett.*, *68*, 3653-3659, 1992.

Savic, M., and A. M. Ziolkowski, "Numerical modeling of elastodynamic radiation and scattering", in *64th Ann. Internat. Mtg., Soc. Expl. Geophys., Expanded Abstracts*, pp. 1294-1297, SEG, Tulsa, 1994.

Schoenberg, M., Elastic wave behavior across linear slip interfaces, *J. Acoust. Soc. Am.*, *68*, 1516-1521, 1980.

Selvadurai, A. P. S., and G. Z. Voyiadjis (Eds.), *Mechanics of Material Interfaces*, Elsevier, new York, 1986.

Tessmer, E., D. Kessler, D. Kosloff, and A. Behle, Multidomain Chebyshev-Fourier method for the solution of the equations of motion of dynamic elasticity, *J. Comput. Phys.*, *100*, 355-363, 1992.

van der Hijden,J. H. M. T., and F. L. Neerhoff, Scattering of elastic waves by a plane crack of finite width, *J. Appl. Mech.*, *51*, 646-651, 1984.

Wills, P. B., D. C. DeMartini, H. J. Vinegar, J. Shlyapobersky, W. F. Deeg, J. C. Woerpel, C. E. Fix, G. G. Sorrells , and R. G. Adair, Active and passive seismic imaging of a hydraulic fracture in diatomite, *Leading Edge*, *11*, 15-22, 1992.

J. M. Carcione, Osservatorio Geofisico Sperimentale, P.O. Box 2011 Opicina, 34016 Trieste, Italy. (Fax +39 40 327307; e-mail: carcione@gems755.ogs.trieste.it)

(Received November 8, 1995; revised May 20, 1996; accepted August 30, 1996.)